Spin excitations in a quantum antiferromagnet with magnetic impurities and vacancies

W. Brenig, Arno P. Kampf

Angaben zur Veröffentlichung / Publication details:

Brenig, W., and Arno P. Kampf. 1991. "Spin excitations in a quantum antiferromagnet with magnetic impurities and vacancies." *Physical Review B* 43 (16): 12914–20. https://doi.org/10.1103/physrevb.43.12914.

Spin excitations in a quantum antiferromagnet with magnetic impurities and vacancies

W. Brenig and A. P. Kampf
Department of Physics, University of California at Santa Barbara, Santa Barbara, California 93106
(Received 9 January 1991)

The two-dimensional antiferromagnetic spin-$\frac{1}{2}$ Heisenberg model on a square lattice is considered in the presence of randomly distributed vacancies and magnetic impurities. We calculate the configurationally averaged spin excitations of the system in the limit of small impurity concentrations. We apply linear spin-wave theory to the host and use the exact T matrix for the impurity sites. Results for the spin-wave spectrum are presented. These include resonant scattering effects, the renormalized spin-wave dispersion, and the spin-wave damping.

I. INTRODUCTION

The common feature of all the high-T_c cuprate superconductors is the presence of two-dimensional CuO_2 planes. Their electronic properties are attributed to holes that are doped into hybridized O $2p_{x,y}$ and Cu $3d_{x^2-y^2}$ orbitals in these planes. For the undoped parent compounds, it is widely accepted to describe the relevant electronic states of these planes in terms of the so-called Mott-Hubbard insulator. In the insulating state, the low-energy, electronic degrees of freedom are essentially reduced to localized spins $\frac{1}{2}$, arising from the $3d_{x^2-y^2}$ antibonding orbitals, which are exactly half-filled in this case. The spins are coupled via the antiferromagnetic exchange interaction. The magnetic properties of these systems are well described by a two-dimensional (2D) Heisenberg quantum antiferromagnet.[1,2] One of the keys to an understanding of the cuprate superconductors may be the interplay between the antiferromagnetic background and the mobile carriers, which are introduced upon doping. This includes the rapid destruction of long-range antiferromagnetic order as a function of doping, which is followed by the onset of superconductivity at intermediate hole concentrations.

From the above, it is evident that investigations of the 2D spin system will contribute to a better understanding of the cuprates. Current topics in this field include quantum effects in the ground state and the excitation spectrum of the pure two-dimensional Heisenberg antiferromagnet.[3,4] In this paper, we will focus on a different aspect, namely, the response of the spin system to a random distribution of magnetic defects and *static* holes that are introduced into the CuO_2 planes. The latter case is of direct experimental interest, as the substitution of nonmagnetic Zn, or Al and Ga (Ref. 5) for Cu in $YBa_2Cu_3O_7$ (Refs. 6 and 7) or La_2CuO_4 (Refs. 5 and 8) samples provides explicit examples for static holes. In addition, the problem of *arbitrary* spin-$\frac{1}{2}$ magnetic impurities in a 2D antiferromagnet is also included in the model we introduce in Sec. II, and it is complementary to the earlier treatment of magnetic impurities in 3D ferromagnets.[9,10] In addition, the problem of randomly distributed vacancies in the Heisenberg antiferromagnet is interesting because the vacancies may be viewed as mobile carriers in the limit of a vanishing bandwidth. Recently, Bulut *et al.*[11] have studied the vacancy problem for a *single* vacancy introduced into the 2D square lattice. They focused on the spin correlations in the immediate neighborhood of the vacancy and compared results obtained within linear spin-wave (LSW) theory to exact diagonalization studies on small clusters. They find LSW to be surprisingly accurate and show, e.g., that the magnetization on sites next to the vacancy is actually enhanced relative to the pure host value.

The paper is organized as follows. In Sec. II, we introduce the model and apply the LSW theory to derive the spin excitations from Dyson's equation for the spin-wave propagator as outlined in Sec. III. To account for the disorder, we perform a configurational average over the impurity positions. In the limit of small defect concentrations, the self-energy is calculated from the single impurity scattering T matrix. In particular, the real space transform of the T matrix can be used to evaluate the spin-correlation functions, which were considered in Ref. 11 for a nearest-neighbor site of a vacancy. In Sec. IV we present our results for the spin-wave spectrum at various defect concentrations and different coupling strengths. The spectra contain typical resonance features reflecting the local symmetry of the impurity potential. Additionally, we discuss the spin-wave damping and a nontrivial renormalization of the spin-wave dispersion due to resonant scattering. We conclude in Sec. V.

II. THE MODEL

The aim of this paper is to describe the spin excitations of a perturbed two-dimensional Heisenberg quantum spin-$\frac{1}{2}$ antiferromagnet. The perturbation we are interested in consists of a random distribution of defect spins on the sites of the 2D square lattice. These defect spins are coupled to the pure host spins by an exchange energy $J-\tilde{J}$, where J is the unperturbed coupling constant. The symmetry of the perturbation is assumed to be that of the square lattice. For the Hamiltonian, we follow the standard procedure and perform a sublattice rotation.[12] This amounts to transforming all spins on *one* of the two sublattices of the antiferromagnet by $S^{\pm} \rightarrow S^{\mp}$

and by $S^z \rightarrow -S^z$. The resulting Hamiltonian is given by

$$H = H_{\rm AFM} + H_{\rm imp} ,$$

$$H_{\rm AFM} = \frac{J}{2} \sum_{\langle ij \rangle} \left[-S_i^z S_j^z + \frac{1}{2}(S_i^+ S_j^+ + S_i^- S_j^-) \right] ,$$

$$H_{\rm imp} = -\frac{\tilde{J}}{2} \sum_{\mathbf{R}_l} \sum_{j(l)} \left[-S_l^z S_j^z + \frac{1}{2}(S_l^+ S_j^+ + S_l^- S_j^-) \right] . \quad (2.1)$$

Here $H_{\rm AFM}$ is the Hamiltonian of the pure host. The summation $\langle ij \rangle$ is assumed to range over all next-nearest neighbor *bonds* of the square lattice. The lattice vectors $\mathbf{R}_l$ in the perturbing Hamiltonian $H_{\rm imp}$ are the random positions of the impurity sites. The index $j(l)$ represents the four next-nearest neighbors of the impurity. We define the concentration of the defects by $c = (1/N)\sum_{\mathbf{R}_l}$, where N is the total number of lattice sites. For $J = \tilde{J}$, the impurity spins are decoupled from the lattice, thus, leading to effective vacancies within the host.

The spin excitations of the Hamiltonian in Eq. (2.1) will be evaluated within the LSW theory.[13] Although a *quantitative* description of the spin dynamics of two-dimensional spin-$\frac{1}{2}$ antiferromagnets requires a better treatment, it is well accepted that the LSW theory provides a good description of their *qualitative* features.[4] Within the LSW approach, the momentum space representation of Eq. (2.1), apart from irrelevant additive constants, is found to be

$$H = \frac{J}{2} \sum_{\mathbf{k}} \hat{\mathbf{A}}^\dagger(\mathbf{k}) \hat{\mathbf{E}}(\mathbf{k}) \hat{\mathbf{A}}(\mathbf{k}) - \frac{\tilde{J}}{8N} \sum_{\mathbf{R}_l, \mathbf{k}, \mathbf{k}', j} e^{i\mathbf{R}_l \cdot (\mathbf{k}-\mathbf{k}')} \hat{\mathbf{A}}^\dagger(\mathbf{k}) \hat{\mathbf{v}}_j^\dagger(\mathbf{k}) \hat{\mathbf{v}}_j(\mathbf{k}') \hat{\mathbf{A}}(\mathbf{k}') . \quad (2.2)$$

Above, we have used that the coordination number of the square lattice is 4, and that the spin quantum number s is equal to $\frac{1}{2}$. The vectors $\mathbf{k}$ label points in the reciprocal space. Note that due to the sublattice rotation, the Brillouin zone is determined by the Brillouin zone of the square lattice, i.e, $k_x, k_y \in [-\pi/2a, \pi/2a]$, where a is the lattice constant, and not by the magnetic Brillouin zone. In Eq. (2.2), we introduced a 2×2 matrix notation. The operator vector $\hat{\mathbf{A}}(\mathbf{k})$ is defined by

$$\hat{\mathbf{A}}(\mathbf{k}) = \begin{bmatrix} a_{\mathbf{k}} \\ a_{-\mathbf{k}}^\dagger \end{bmatrix} , \quad (2.3)$$

where the so-called spin-wave operators $a_{\mathbf{k}}^\dagger$ and $a_{\mathbf{k}}$ are the $\mathbf{k}$-space transforms of the linearized Holstein-Primakoff representations of the spin operators.[14] The matrix $\hat{\mathbf{E}}(\mathbf{k})$ is given by

$$\hat{\mathbf{E}}(\mathbf{k}) = \begin{bmatrix} 1 & \gamma_{\mathbf{k}} \\ \gamma_{\mathbf{k}} & 1 \end{bmatrix} ,$$

$$\gamma_{\mathbf{k}} = \tfrac{1}{2}[\cos(ak_x) + \cos(ak_y)] . \quad (2.4)$$

Finally, the impurity part of the Hamiltonian contains the matrix $\hat{\mathbf{v}}_j(\mathbf{k})$. It is given by

$$\hat{\mathbf{v}}_j(\mathbf{k}) = \begin{bmatrix} 1 & e^{i\mathbf{k}\cdot\mathbf{r}_j} \\ e^{i\mathbf{k}\cdot\mathbf{r}_j} & 1 \end{bmatrix} , \quad (2.5)$$

where $\mathbf{r}_j$ are the vectors pointing from an impurity site to its four next-nearest neighbors. For further reference, we assume $j = 1,2,3,4$ to label these sites in a counterclockwise direction. Note that within the above representation the impurity potential as given by Eq. (2.2) is factorized regarding the dependence on $\mathbf{k}$ and $\mathbf{k}'$.

III. THE SPIN EXCITATIONS

In this section, we solve for the relevant Green's function of the Hamiltonian given by Eq. (2.2). As usual, our aim will *not* be to evaluate this Green's function for a given, fixed set of impurity positions. Instead, what we are interested in is the Green's function that will arise from an ensemble average over randomly located defects at a given concentration c. We apply the finite temperature formalism and consider the imaginary time propagator matrix

$$\mathcal{G}^{\alpha\beta}(\mathbf{k},\tau) = -\langle T_\tau \{ A^\alpha(\mathbf{k},\tau)[A^\dagger(\mathbf{k},0)]^\beta \} \rangle . \quad (3.1)$$

The Greek indices refer to the components of the vector defined in Eq. (2.3). The brackets $\langle \cdots \rangle$ imply not only the trace over the statistical operator, but also, a configurational average over the impurity positions. The latter will be achieved using the standard method of Refs. 15 and 16. Within this approach the averaged dressed spin-wave propagator is obtained by the Dyson equation for $\hat{\mathcal{G}}(\mathbf{k},\omega_n)$,

$$\hat{\mathcal{G}}(\mathbf{k},\omega_n) = \hat{\mathcal{G}}_0(\mathbf{k},\omega_n) + \hat{\mathcal{G}}_0(\mathbf{k},\omega_n)\hat{\Sigma}(\mathbf{k},\omega_n)\hat{\mathcal{G}}(\mathbf{k},\omega_n) . \quad (3.2)$$

Here $\hat{\Sigma}(\mathbf{k},\omega_n)$ is the self-energy for spin waves scattering off impurities represented by the perturbing part $H_{\rm imp}$ of Eq. (2.2). Note that due to the impurity averaging, the self-energy is $\mathbf{k}$ diagonal. The bosonic Matsubara frequencies are given by $\omega_n = 2\pi n T$, where T is the temperature and n is an integer number. The matrix elements of the unperturbed Green's function $\hat{\mathcal{G}}_0(\mathbf{k},\omega_n)$ are determined by[12]

$$\mathcal{G}_0^{11}(\mathbf{k},\omega_n) = \mathcal{G}_0^{22}(\mathbf{k},-\omega_n) = \frac{J + i\omega_n}{(i\omega_n)^2 - (\varepsilon_{\mathbf{k}})^2}$$

$$\mathcal{G}_0^{12}(\mathbf{k},\omega_n) = \mathcal{G}_0^{21}(\mathbf{k},\omega_n) = \frac{-\gamma_{\mathbf{k}}}{(i\omega_n)^2 - (\varepsilon_{\mathbf{k}})^2} . \quad (3.3)$$

The unperturbed spin-wave dispersion is given by $\varepsilon_{\mathbf{k}} = J(1-\gamma_{\mathbf{k}}^2)^{1/2}$. The bare $\hat{\mathcal{G}}_0(\mathbf{k},\omega_n)$ is diagonalized in the standard way by the Bogoliubov transformation.[12]

To determine the self-energy $\hat{\Sigma}(\mathbf{k},\omega_n)$, we introduce the second approximation used in this paper. Namely, we restrict ourselves to the dilute limit. In this limit, only diagrams to lowest, linear order in the defect concentration have to be included within the averaging procedure, as shown in Fig. 1. This is equivalent to treating the on-site scattering process exactly and neglecting all correlations between different impurity sites. The resulting integral equation will become algebraic because of the factorization of the impurity scattering potential into a $\mathbf{k}$-

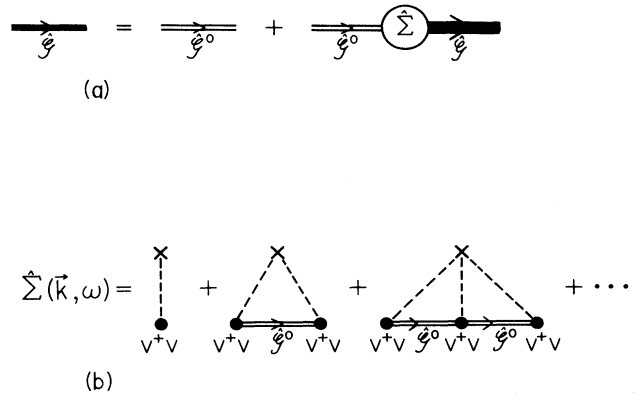

FIG. 1. (a) The Dyson equation for the spin-wave propagator $\hat{\mathcal{G}}$, $\hat{\mathcal{G}}_0$ is the bare propagator, and $\hat{\Sigma}$ is the self-energy. (b) Diagrams for the self-energy. Scattering off a specific impurity is represented by a full circle attached to a dashed line. Configurational averaging is symbolized by a cross.

and a $\mathbf{k}'$-dependent part. We obtain

$$\hat{\Sigma}(\mathbf{k},\omega_n)=-c\frac{\tilde{J}}{4}\sum_{jl}\hat{\mathbf{v}}_j^{\dagger}(\mathbf{k})\hat{\mathbf{t}}_{jl}(\omega_n)\hat{\mathbf{v}}_l(\mathbf{k}) ,$$

$$\hat{\mathbf{t}}_{jl}(\omega_n)=\hat{\mathbf{1}}\delta_{jl}+\sum_m\hat{\mathbf{t}}_{0,jm}(\omega_n)\hat{\mathbf{t}}_{ml}(\omega_n) , \tag{3.4}$$

$$\hat{\mathbf{t}}_{0,jm}(\omega_n)=-\frac{\tilde{J}}{4}\frac{1}{N}\sum_{\mathbf{k}}\hat{\mathbf{v}}_j(\mathbf{k})\hat{\mathcal{G}}_0(\mathbf{k},\omega_n)\hat{\mathbf{v}}_m^{\dagger}(\mathbf{k}) .$$

The remaining equation for the exact single-site T matrix $\hat{\mathbf{t}}_{jl}(\omega_n)$ can be diagonalized with respect to the indices $j,l=1,2,3,4$ for the sites next to the impurity, by transforming into S-, P-, and D-symmetric channels with respect to the scattering site. After straightforward algebraic manipulations, we find

$$\hat{\Sigma}(\mathbf{k},\omega_n)=-c\frac{\tilde{J}}{4}\sum_{I=S,P_1,P_2,D}\hat{\mathbf{w}}_I^{\dagger}(\mathbf{k})\hat{\mathbf{t}}_I(\omega_n)\hat{\mathbf{w}}_I(\mathbf{k}) . \tag{3.5}$$

Above, we have introduced the S, P, and D representations of the single-site scattering T matrices. Within our 2×2 formulation, these matrices are found to be diagonal. For the different channels, their elements are given by

$$t_S^{11}(\omega_n)=t_S^{22}(-\omega_n)=\frac{1}{1+\tilde{J}\left[G_{00}(\omega_n)+2F_{10}(\omega_n)+\frac{1}{4}\sum_j G_{j1}(-\omega_n)\right]}$$

$$t_{P_1}^{11}(\omega_n)=t_{P_1}^{22}(-\omega_n)=\frac{1}{1+(\tilde{J}/4)[G_{11}(-\omega_n)-G_{31}(-\omega_n)]}$$

$$t_D^{11}(\omega_n)=t_D^{22}(-\omega_n)=\frac{1}{1+(\tilde{J}/4)\left[\sum_j(-)^{j+1}G_{j1}(-\omega_n)\right]} . \tag{3.6}$$

The irreducible parts of the T matrices in Eq. (3.6) are expressed in terms of the lattice Green's functions $G_{ij}(\omega_n)$ and $F_{ij}(\omega_n)$. These are defined as the Fourier transforms of the diagonal and off-diagonal elements of the unperturbed spin-wave propagators, respectively,

$$G_{ij}(\omega_n)=\frac{1}{N}\sum_{\mathbf{k}}e^{i\mathbf{k}\cdot(\mathbf{r}_i-\mathbf{r}_j)}\mathcal{G}_0^{11}(\mathbf{k},\omega_n) ,$$

$$F_{ij}(\omega_n)=\frac{1}{N}\sum_{\mathbf{k}}e^{i\mathbf{k}\cdot(\mathbf{r}_i-\mathbf{r}_j)}\mathcal{G}_0^{12}(\mathbf{k},\omega_n) , \tag{3.7}$$

All of the lattice Green's functions are related to elliptic integrals of the first and the second kind.[17,18] Explicit expressions for the corresponding causal Green's functions are evaluated in the Appendix A. Note that the matrices $\hat{\mathbf{t}}_I(\omega_n)$ are diagonal because all lattice Green's functions that appear in the off-diagonal elements of the irreducible parts of the $\hat{\mathbf{t}}_I(\omega_n)$'s are zero.

The matrices $\hat{\mathbf{w}}_I^{\dagger}(\mathbf{k})$ in Eq. (3.5) are the S-, P-, and D-like linear combinations of the $\hat{\mathbf{v}}_i^{\dagger}(\mathbf{k})$ matrices, respectively. They are given by

$$\hat{\mathbf{w}}_S(\mathbf{k})=\tfrac{1}{2}[\hat{\mathbf{v}}_1(\mathbf{k})+\hat{\mathbf{v}}_2(\mathbf{k})+\hat{\mathbf{v}}_3(\mathbf{k})+\hat{\mathbf{v}}_4(\mathbf{k})] ,$$

$$\hat{\mathbf{w}}_{P_{\frac{1}{2}}}(\mathbf{k})=\tfrac{1}{2}[\hat{\mathbf{v}}_1(\mathbf{k})\pm\hat{\mathbf{v}}_2(\mathbf{k})-\hat{\mathbf{v}}_3(\mathbf{k})\mp\hat{\mathbf{v}}_4(\mathbf{k})] ,$$

$$\hat{\mathbf{w}}_D(\mathbf{k})=\tfrac{1}{2}[\hat{\mathbf{v}}_1(\mathbf{k})-\hat{\mathbf{v}}_2(\mathbf{k})+\hat{\mathbf{v}}_3(\mathbf{k})-\hat{\mathbf{v}}_4(\mathbf{k})] . \tag{3.8}$$

Using Eq. (2.5), it is evident that the elements of the above 2×2 matrices $\hat{\mathbf{w}}_I(\mathbf{k})$ consist of the usual square harmonics, i.e., $\cos(ak_x)\pm\cos(ak_y)$ and $\sin(ak_x)\pm\sin(ak_y)$. In contrast to the $\hat{\mathbf{t}}_I(\omega_n)$'s the off-diagonal elements of the coupling matrices $\hat{\mathbf{w}}_I(\mathbf{k})$ are nonzero. Thus, the self-energy matrix $\hat{\Sigma}(\mathbf{k},\omega_n)$ is not diagonal in the above representation.

Before turning to the discussion, we would like to point out one particular property of the S channel for the case of $\tilde{J}=J$. With the expressions given in the Appendix and with Eq. (3.6), the causal scattering T matrix, which is obtained from the analytic continuation of $\hat{\mathbf{t}}_S(\omega_n)$ to the real axis, can be evaluated to be

$$t_S^{11}(\omega)=t_S^{22}(-\omega)=\frac{1}{\tilde{J}\omega[\omega G_{00}(\omega)-1]+1-\tilde{J}}$$

$$=\frac{1}{\omega[\omega G_{00}(\omega)-1]}\quad\text{for }\tilde{J}=J , \tag{3.9}$$

where all energies are measured in units of J. Equation (3.9) shows that the self-energy will develop a $1/\omega$ singularity at small ω for $\tilde{J}\to J$. This is related to the fact that the S-like scattering states of the spin waves have a nonzero projection onto the states of the central spin. If $\tilde{J}=J$, this spin is completely decoupled from all other spins. Thus, the relevant spin operator commutes with the Hamiltonian leading to a zero-frequency mode.

IV. RESULTS AND DISCUSSION

Given the self-energy as calculated from the single-site scattering T matrix, we can invert Dyson's equation, Eq. (3.2), to obtain the configuration averaged spin-wave propagator matrix. Its components contain all the information about the renormalized spin excitations. Explicit comparison to the spin-wave spectrum of the pure host is conveniently carried out in an operator representation that diagonalizes the Hamiltonian in the absence of any impurities. This is achieved introducing the operators $b_{\mathbf{k}}^{\dagger}$ and $b_{\mathbf{k}}$ by the canonical Bogoliubov transformation

$$\begin{bmatrix} b_{\mathbf{k}} \\ b_{-\mathbf{k}}^{\dagger} \end{bmatrix} = \begin{bmatrix} u_{\mathbf{k}} & -v_{\mathbf{k}} \\ -v_{\mathbf{k}} & u_{\mathbf{k}} \end{bmatrix} \hat{A}_{\mathbf{k}} , \tag{4.1}$$

with the coefficients $u_{\mathbf{k}}$ and $v_{\mathbf{k}}$ determined from

$$u_{\mathbf{k}}^2 = \frac{1}{2}\left[\frac{1}{(1-\gamma_{\mathbf{k}}^2)^{1/2}}+1\right], \quad v_{\mathbf{k}}^2 = 1-u_{\mathbf{k}}^2 . \tag{4.2}$$

For the remainder of the discussion, we focus on the 11-component of the spin-wave propagator $\mathcal{G}_b^{11}(\mathbf{k},\omega_n)$ in the b representation for different impurity concentrations. After analytic continuation to the real frequency axis, the spectral function of $\mathcal{G}_b(\mathbf{k},\omega)$ is given by

$$\begin{aligned} A(\mathbf{k},\omega) &= -\frac{1}{\pi}\,\mathrm{Im}\mathcal{G}_b^{11}(\mathbf{k},\omega) \\ &= -\frac{1}{\pi}\,\mathrm{Im}\frac{1}{\omega-\varepsilon_{\mathbf{k}}-\Sigma_b^{11}(\mathbf{k},\omega)+[\Sigma_b^{12}(\mathbf{k},\omega)]^2/[\omega+\varepsilon_{\mathbf{k}}+\Sigma_b^{22}(\mathbf{k},\omega)]} . \end{aligned} \tag{4.3}$$

Here, $\hat{\Sigma}_b(\mathbf{k},\omega)$ is the canonical transform of $\hat{\Sigma}(\mathbf{k},\omega)$. In the pure host limit $c=0$, the self-energy vanishes, and $A(\mathbf{k},\omega)$ is a single δ function at the spin-wave energy $\varepsilon_{\mathbf{k}}$ for given momentum $\mathbf{k}$. At small but finite c, the energies of the spin waves are shifted, and they acquire a finite lifetime in the forward momentum channel due to repeated scattering from individual impurities.

In Figs. 2 and 3, we plot two examples for $\mathrm{Im}\mathcal{G}_b^{11}(\mathbf{k},\omega)$ or, equivalently, the spectral function at fixed momentum $\mathbf{k}=(\pi/4a,\pi/4a)$ as a function of frequency. In Fig. 2, we have chosen a case where the impurity spin is coupled to its neighboring spins with half of the pure host value, i.e., $\tilde{J}=J/2$. The spin-wave peak moves to lower energies with increasing impurity concentration and is considerably broadened. For large enough values of c, additional structure appears in the spectral function, which arises from resonances in the S-, P-, and D-scattering channels at the impurity sites. Due to their local nature,

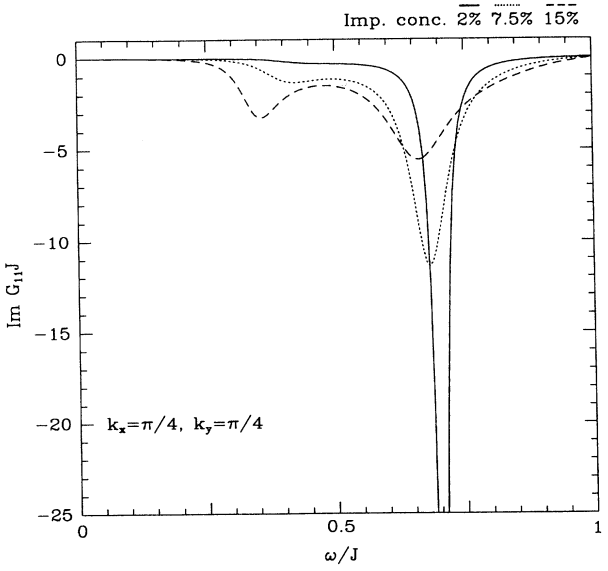

FIG. 2. Imaginary part of the diagonal element of the spin-wave propagator matrix at fixed momentum for various impurity concentrations and $\tilde{J}=J/2$.

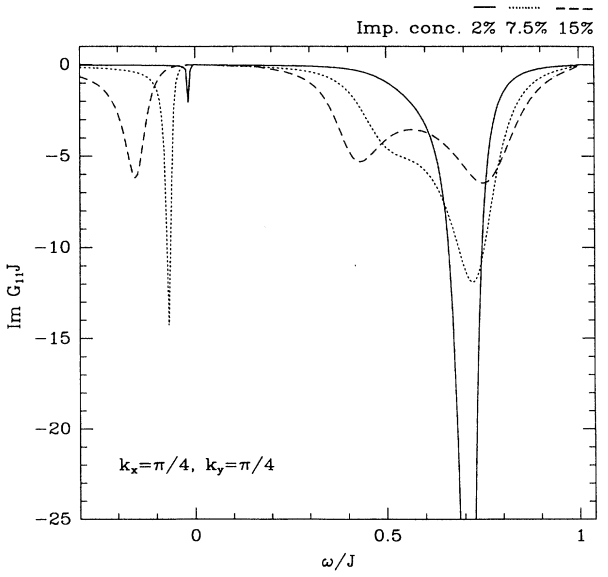

FIG. 3. Same as Fig. 2, for $\tilde{J}=J$.

the energy of these resonances is independent of $\mathbf{k}$. To illustrate the effect on the spin-wave spectrum, we have chosen the momentum such that the unperturbed excitation energy lies close to one of these resonances. Essentially no spectral weight appears outside the band $0<\omega<J$. Figure 3 shows the behavior of the spectral function for $J=\tilde{J}$, which corresponds to impurity spins that are decoupled from their surrounding and, thus, act as vacancies. Note that for the momentum chosen in this case the spin-wave peak moves to higher energies with increasing c. However, for the larger defect concentrations greater than or approximately equal to 10%, to which we extend the results of our dilute limit calculation, spin-waves are no longer well defined in the frequency range close to the resonant structures. In fact, in this frequency range both have comparable spectral weight and become hardly distinguishable in the spectral function.

As in all spectra for $J=\tilde{J}$, there is also a sharp peak outside the magnon band near $\omega=0$. Its spectral weight is determined by the defect concentration. This peak arises from the zero-frequency mode of the decoupled free spin at the impurity site as pointed out in connection with the T matrix of Eq. (3.9). For the *exact* impurity-averaged spin-wave spectrum, this would lead to a δ function at $\omega=0$. Our calculation, however, approximates the configurationally averaged Green's function only to leading order in the impurity concentration. As an artifact of this approximate treatment, the "free-spin" pole is shifted away from $\omega=0$. Summing up, higher-order contributions in powers of c would remedy this deficiency.

From the position of the dominant peak in the spectral function $A(\mathbf{k},\omega)$, we can deduce the spin-wave dispersion by mapping out the peak position as a function of momentum. The results are collected in Fig. 4 for momenta along the diagonal of the Brillouin zone with $k_x=k_y$. The dispersion of the pure system is included as a reference. At long wavelengths, the dispersion maintains its linear $\mathbf{k}$ dependence with a reduced spin-wave velocity v_s. For low-impurity concentrations, v_s is approximately given by $v_s=(1-\alpha c)J/(2)^{1/2}$. From our analysis, we find $\alpha\approx 3.1$. For concentrations of $c\gtrsim 5\%$, corrections quadratic in c modify this result. Close to the top of the magnon band, the spin-wave energies are shifted to higher energies. This is an immediate consequence of the presence of the local S, P, and D resonances appearing at intermediate energies. As mentioned above, for larger concentrations, the spin waves and the resonances are not clearly separated in this energy range. This explains the discontinuity in the curves of Fig. 4 reflecting the criterion to plot the position of the peak carrying most of the spectral weight in $A(\mathbf{k},\omega)$. Outside the resonance regime, the identification of the spin-wave peak is unique. Figure 5 shows the width of the peak as defined by the imaginary part of the self-energy at the peak position, which is mapped out in Fig. 4. It is a measure of the relaxation rate out of a given momentum state due to impurity scattering. The damping vanishes at the magnon band edges, i.e., for $\omega=0$ and $\omega=J$, and it is largest for intermediate values close to the resonant frequencies.

Finally, we would like to mention a simple way to remove the low-frequency spectral weight that appears for $\tilde{J}=J$ due to the free-spin mode. For that purpose, we have treated a generalization of our model by adding a term $H_B=-\mu B\sum_{\mathbf{R}_l}S_l^z$ to the Hamiltonian equation (2.1). Here, B is a fictitious magnetic field that is used to freeze out the vacancy spin carrying the magnetic moment μ. We find[19] the P and D channels of the self-energy to be unchanged, but there is one additional channel which mixes with the former S channel. In the limit of $\mu B\gg J$, the free-spin excitation is shifted to high energy. In this

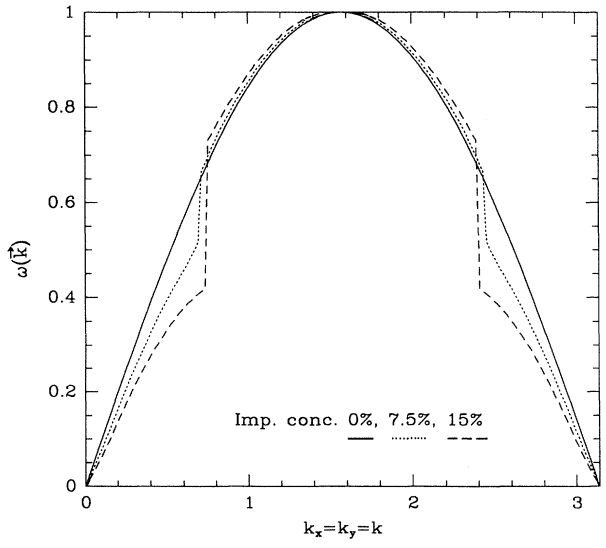

FIG. 4. Spin-wave dispersion for various impurity concentrations. The dispersion for the pure host is included as a reference.

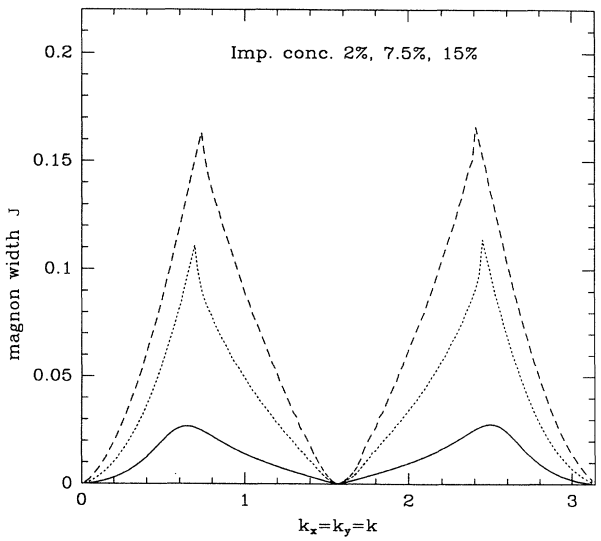

FIG. 5. Spin-wave damping for various impurity concentrations.

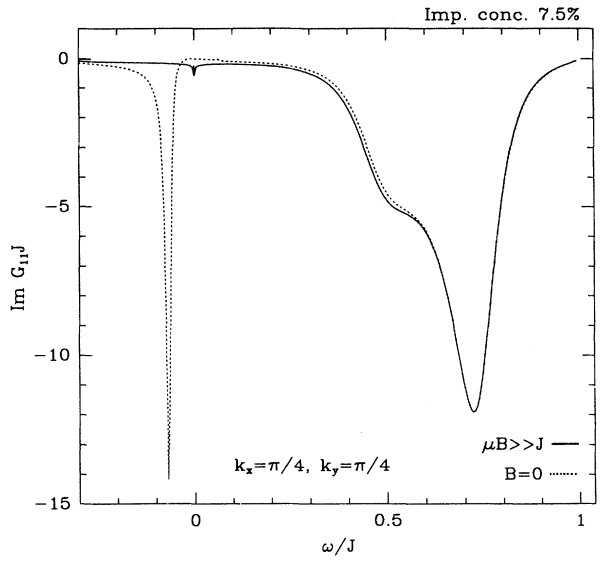

FIG. 6. Imaginary part of the diagonal element of the spin-wave propagator matrix for finite B field. Comparison of "frozen" vs "free" defect spin in the case of $\bar{J}=J$.

case, and for $\omega \ll \mu B$, the scattering T matrix in the S channel as compared with Eq. (3.9) changes into

$$t_S^{11}(\omega)=t_S^{22}(-\omega)\overset{\bar{J}=J}{=}\frac{G_{00}(\omega)}{\omega G_{00}(\omega)-1} . \tag{4.4}$$

The above expression no longer has the $1/\omega$ singularity. This is shown in Fig. 6, where the dotted curve refers to the corresponding spectrum for $B=0$. The rest of the spectrum and in particular the position of the spin-wave peak remain unchanged.

V. CONCLUSION

To summarize, we have studied the influence of magnetic impurities and vacancies on the spin excitations of a 2D quantum antiferromagnet. We applied LSW theory and evaluated the spin-wave propagator to leading order in the defect concentration. Our results for the renormalization of the spin-wave spectrum should be accessible to neutron scattering and other experiments that probe magnetic excitations of the high-T_c compounds with respect to impurities and vacancies introduced into the CuO_2 planes. Comparing our findings with the impact of *mobile* holes on the magnetic correlations in the planes, in particular, the spin-wave stiffness, it is obvious that static holes are less effective in suppressing magnetic order. This is due to the mobile holes disrupting the antiferromagnetic order via the direct correlations between their motion and the spin background. It is only in the limit of very low doping concentration, where localization effects play a role, that our results may be relevant for hole-doped samples as well. Finally, we would like to remark that our approach could be extended to include corrections beyond LSW theory and contributions due to higher orders in the defect concentration as well as their interplay.

Note added in proof. After completing this work we became aware of an additional publication on *single* defects in two-dimensional quantum antiferromagnets, treating the case of one isolated ferromagnetic bond.[21]

ACKNOWLEDGMENTS

We thank N. Bulut, H. Monien, D. J. Scalapino, and J. R. Schrieffer for helpful discussions. This work was supported by the National Science Foundation under Grant No. DMR 89-18307 and EPRI Grant No. RP-8009-18. One of us (W.B.) gratefully acknowledges support by the Max-Planck-Gesellschaft.

APPENDIX

The calculation of the scattering T matrix in Sec. III involves the evaluation of the pure host Green's functions $G_{ij}(\omega_n)$ and $F_{ij}(\omega_n)$, as defined in Eq. (3.7) and, in particular, their analytic continuation to the real frequency axis. The analytic properties of the host Green's functions are intimately related to those of the lattice Green's function of the two-dimensional square lattice.[17] We enumerate counterclockwise the nearest-neighbor sites of an arbitrary central site $\mathbf{r}_0$ by $\mathbf{r}_1,\mathbf{r}_2,\mathbf{r}_3,\mathbf{r}_4$. For these five lattice sites, there are four nonvanishing independent host Green's functions, which we denote by G_{00}, F_{10}, G_{21}, and G_{31}. Measuring energies in units of the exchange energy J, we restrict ourselves to frequencies $|\omega|\leq 1$ inside the magnon band since the host Green's functions are purely real outside the magnon band and, hence, no spectral weight appears for $|\omega|\geq 1$. The four (causal) Green's functions are given by[18,20] (for $-1<\omega<1$):

$$G_{00}(\omega)=-\frac{2}{\pi}\left[\frac{1+\omega}{1-\omega}\right]^{1/2}\{K[(1-\omega^2)^{1/2}]+iK(|\omega|)\} , \tag{A1}$$

$$F_{10}(\omega)=(\omega-1)G_{00}(\omega)-1 , \tag{A2}$$

$$G_{21}(\omega)=-\frac{2}{\pi}\left[\frac{1+\omega}{1-\omega}\right]^{1/2}\{K[(1-\omega^2)^{1/2}]-2E[(1-\omega^2)^{1/2}]-i[K(|\omega|)-2E(|\omega|)]\} , \tag{A3}$$

$$G_{31}(\omega)=(3-4\omega^2)G_{00}(\omega)+4(1+\omega)-2G_{21}(\omega) . \tag{A4}$$

K and E denote the complete elliptic integrals of the first and second kind. The Green's functions for larger distances can be generated from Eqs. (A1), (A2), and (A3) with the recursion relations of Morita.[18]

[1]S. Chakravarty, B. I. Halperin, and D. R. Nelson, Phys. Rev. Lett. **60**, 1057 (1988).
[2]R. J. Birgeneau and G. Shirane, in *Physical Properties of High Temperature Superconductors,* edited by D. M. Ginsberg (World Scientific, Singapore, 1989).
[3]K. W. Becker, H. Won, and P. Fulde, Z. Phys. Cond. Matter B **75**, 335 (1989).
[4]J. D. Reger and A. P. Young, Phys. Rev. B **37**, 5978 (1988).
[5]G. Xiao, M. Z. Cieplak, J. Q. Xiao, and C. L. Chien, Phys. Rev. B **42**, 8752 (1990).
[6]G. Xiao, M. Z. Cieplak, A. Garvin, F. H. Streitz, A. Bakhshai, and C. L. Chien, Phys. Rev. Lett. **60**, 1446 (1988).
[7]J. T. Markert, V. Dalichaouch, and M. B. Maple, *Physical Properties of High Temperature Superconductors* (Ref. 2), p. 265.
[8]A. M. Finkel'stein, V. E. Kataev, E. F. Kukovitkii, and G. B. Teitel'baum, Physica C **168**, 370 (1990).
[9]H. Ishii, J. Kanamori, and T. Nakamura, Prog. Theor. Phys. **33**, 795 (1965).
[10]Y.-L. Wang and H. Callen, Phys. Rev. **160**, 358 (1967).
[11]N. Bulut, D. Hone, D. J. Scalapino, and E. Y. Loh, Phys. Rev. Lett. **62**, 2192 (1989).
[12]D. C. Mattis, *The Theory of Magnetism I* (Springer, Berlin, 1988).
[13]P. W. Anderson, Phys. Rev. **86**, 358 (1952).
[14]T. Holstein and H. Primakoff, Phys. Rev. **58**, 1048 (1940).
[15]S. Doniach and E. H. Sondheimer, *Green's Functions for Solid State Physicists* (Benjamin Cummings, Reading, MA, 1982).
[16]A. A. Abrikosov, L. P. Gorkov, and I. E. Dzyaloshinski, *Methods of Quantum Field Theory in Statistical Physics* (Dover, New York, 1975).
[17]S. Katsura and S. Inawashiro, J. Math. Phys. **12**, 1622 (1971).
[18]T. Morita, J. Math. Phys. **12**, 1744 (1971).
[19]W. Brenig and A. P. Kampf (unpublished).
[20]J. Spanier and K. B. Oldham, *The Atlas of Functions* (Hemisphere, Washington, 1987), p. 609.
[21]K. J. B. Lee and P. Schlottmann, Phys. Rev. B **42**, 4426 (1990).